# Applications of Displacement Transfer Functions to Deformed Shape Predictions of the GIII Swept-Wing Structure

*Shun-Fat Lung, Ph.D.* and William L. Ko, Ph.D.***

*: Jacobs Technology Incorporation
**: NASA Armstrong Flight Research Center


Structural Dynamics Group, Aerostructures Branch (RS), NASA Armstrong Flight Research Center

# Outline

- Motivations
- Background
- GIII wing load calibration test
- Finite element model correlation
- Displacement Transfer Functions
- DTFs Application
- Results comparisons
- Conclusion

# Motivations

- Validate the accuracy of the displacement transfer functions (DTFs) when applied to the swept-wing structure
- Evaluate real time shape sensing possibility and efficiency to support future flight testing activities for the GIII aircraft
- Evaluate the accuracy of the wing deflection estimation when changing the number of strain stations

# Background

- In June 2003, Helios broke up during flight test due to pitching oscillation under large wing dihedral bending. Therefore, real time wing deformed shape monitoring during flight is needed.

- In 2007, Ko et al developed the Displacement Transfer Functions for transforming surface strain into deflections for wing deformed shape estimations.

- Displacement Transfer Functions have been applied to wing shape predictions of Ikhana and Global Hawk successfully


- In late 2009, NASA Armstrong Flight Research Center [AFRC] acquired a Gulfstream III [G-III] business jet airplane (Gulfstream Aerospace Corporation, Savannah, Georgia) to conduct various research projects

- The current AFRC project utilizing the G-III airplane is the Adaptive Compliant Trailing Edge [ACTE] flap experiment. These unconventional adaptive compliant flap structures developed by FlexSys Inc. (Ann Arbor, Michigan) replaced the conventional Fowler flaps.

- Due to the modification of the control surfaces, extensive ground load tests have been done on the GIII aircraft for the wing load calibration

# GIII Wing Load Calibration

- Due to differences between the ACTE structure and the original Fowler flaps with respect to weight, geometry, and flight-testing conditions, the aerodynamic and inertial loads were expected to be different
- In order to protect the wing structure during flight, load equations were developed using strains loads data from a ground load calibration test. These load equations were integrated in the Mission Control Room for real-time monitoring of the aerodynamic loads during flight. Wing deflected shape under load was also characterized and used to tune existing FEM models of the G-III wing structure.

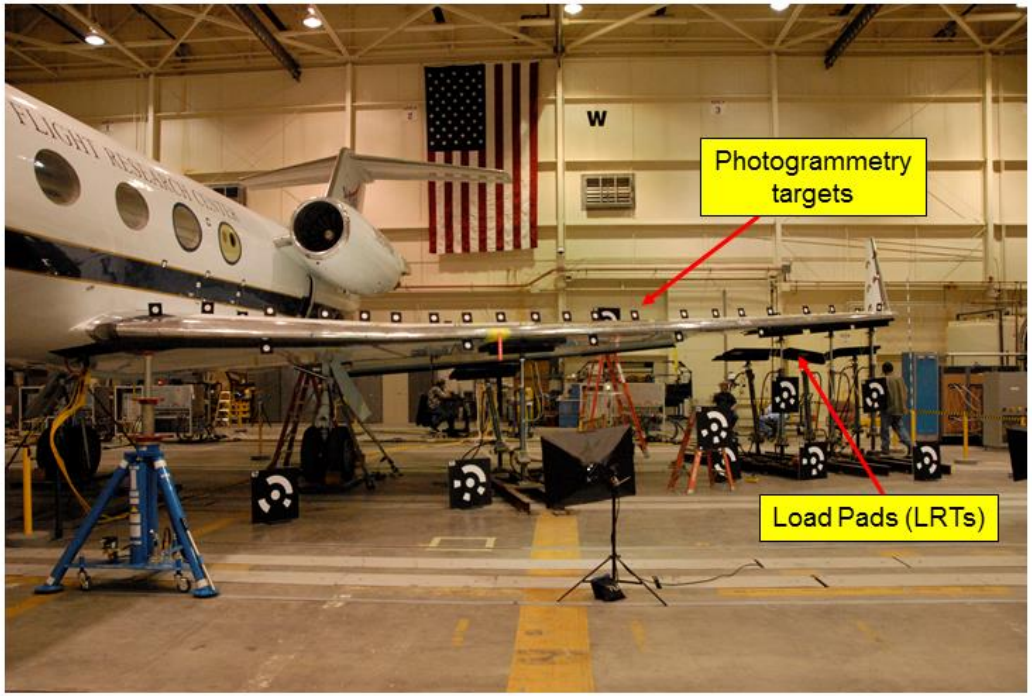


| Load case | Type of loading | Description |
|---|---|---|
| 1 | Shot bags | Outboard loading |
| 3 | Combined | Forward shot and aft hydraulic loading |
| 6 | Combined | Aft shot and forward hydraulic loading |
| 24 | Hydraulic | Maximum loading |

# Finite Element Model Correlations

- Two finite element models
  - Model 1 built from CAD (Top)
  - Model 2 built from Stress Report (Bottom)

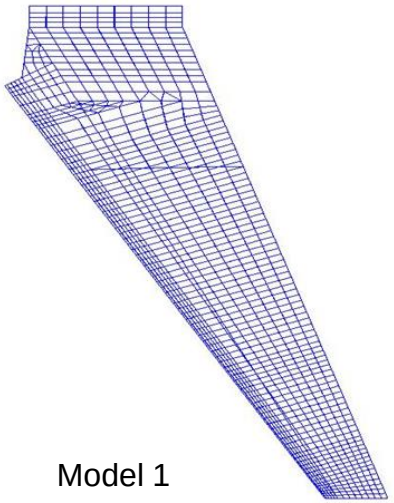

Model 1

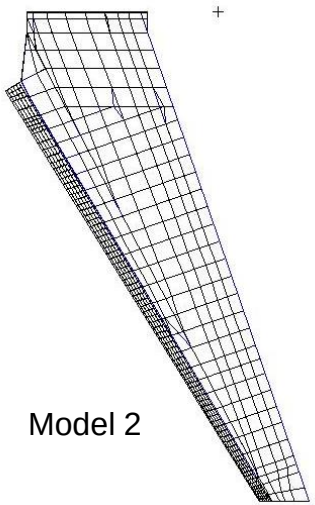

Model 2

Table 1. Finite element model correlations for load case 1.

| String pot | Measured deflection | Wing box model 1 | | Wing box model 2 | |
|---|---|---|---|---|---|
| | | Deflection | Difference, % | Deflection | Difference, % |
| 1 | -1.00 | -0.96 | -4 | -0.98 | -2 |
| 2 | -0.95 | -0.91 | -4 | -0.93 | -2 |
| 3 | -0.44 | -0.43 | -3 | -0.42 | -5 |
| 4 | -0.46 | -0.45 | -2 | -0.44 | -3 |
| 5 | -0.23 | -0.22 | -4 | -0.20 | -11 |
| 6 | -0.21 | -0.20 | -3 | -0.19 | -8 |

Table 2. Finite element model correlations for load case 3.

| LRT | Measured deflection | Wing box model 1 | | Wing box model 2 | |
|---|---|---|---|---|---|
| | | Deflection | Difference, % | Deflection | Difference, % |
| 1 | 1.00 | 0.99 | -1 | 1.01 | 1 |
| 2 | | 0.96 | | | |
| 3 | 0.83 | 0.82 | 0 | 0.83 | 0 |
| 4 | | 0.80 | | | |
| 5 | 0.67 | 0.68 | 1 | 0.64 | -4 |
| 6 | | 0.65 | | | |
| 7 | 0.20 | 0.20 | -3 | 0.15 | -25 |
| 8 | | 0.15 | | | |

# Finite Element Correlations (Cont.)

Table 3. Finite element model correlations for load case 6.

| LRT | Measured deflection | Wing box model 1 | | Wing box model 2 | |
|---|---|---|---|---|---|
| | | Deflection | Difference, % | Deflection | Difference, % |
| 1 | | 1.04 | | | |
| 2 | 1.00 | 1.03 | 3 | 1.07 | 7 |
| 3 | | 0.86 | | | |
| 4 | 0.85 | 0.86 | 2 | 0.88 | 4 |
| 5 | | 0.70 | | | |
| 6 | 0.67 | 0.71 | 5 | 0.68 | 1 |
| 7 | | 0.18 | | | |
| 8 | 0.19 | 0.18 | -9 | 0.16 | -16 |

Table 4. Finite element model correlations for load case 24.

| LRT | Measured deflection | Wing box model 1 | | Wing box model 2 | |
|---|---|---|---|---|---|
| | | Deflection | Difference, % | Deflection | Difference, % |
| 1 | 1.00 | 1.07 | 7 | 1.09 | 9 |
| 2 | 1.00 | 1.05 | 5 | 1.07 | 7 |
| 3 | 0.86 | 0.90 | 4 | 0.90 | 5 |
| 4 | 0.86 | 0.89 | 3 | 0.89 | 4 |
| 5 | 0.70 | 0.74 | 6 | 0.70 | 1 |
| 6 | 0.70 | 0.73 | 4 | 0.69 | -1 |
| 7 | 0.21 | 0.21 | -2 | 0.17 | -21 |
| 8 | 0.17 | 0.18 | 8 | 0.16 | -2 |

# Displacement Theory

- Shifted Lagrangian curvature equation:

$$\frac{1}{R(x)} = \frac{d^2y/dx^2}{\sqrt{1-(dy/dx)^2}} \xrightarrow{\text{Shifting} = (u \to 0) \\ = [(dy/dx)^2 = 0]} \frac{\overbrace{d^2y/dx^2}^{\text{Increased to maintain same } \varepsilon(s)/c(s)}}{\underbrace{\sqrt{1-0}}_{\text{Increased}}} = \frac{d^2y}{\underbrace{dx^2}_{\text{Shifted}}} = \frac{\varepsilon(s)}{c(s)} \qquad (1)$$

- Piece-wise representations:

$$c(x) = c_{i-1} + (c_i - c_{i-1})\frac{x - x_{i-1}}{\Delta l} \qquad (x_{i-1} \le x \le x_i)$$

$$e(x) = e_{i-1} + (e_i - e_{i-1})\frac{x - x_{i-1}}{\Delta l} \qquad (x_{i-1} \le x \le x_i)$$

Slope [integration of (1)]:

$$\tan\theta(x) = \frac{dy}{dx} = \int_{x_{i-1}}^{x} \frac{e(x)}{c(x)}dx + \tan\theta_{i-1} \qquad (2)$$

Deflection [integration of (2)]:

$$y(x) = \underbrace{\int_{x_{i-1}}^{x} \tan\theta(x)dx}_{\text{Integration of slope}} + \underbrace{y_{i-1}}_{\substack{\text{Deflection} \\ \text{at } x_{i-1}}} \qquad (3)$$

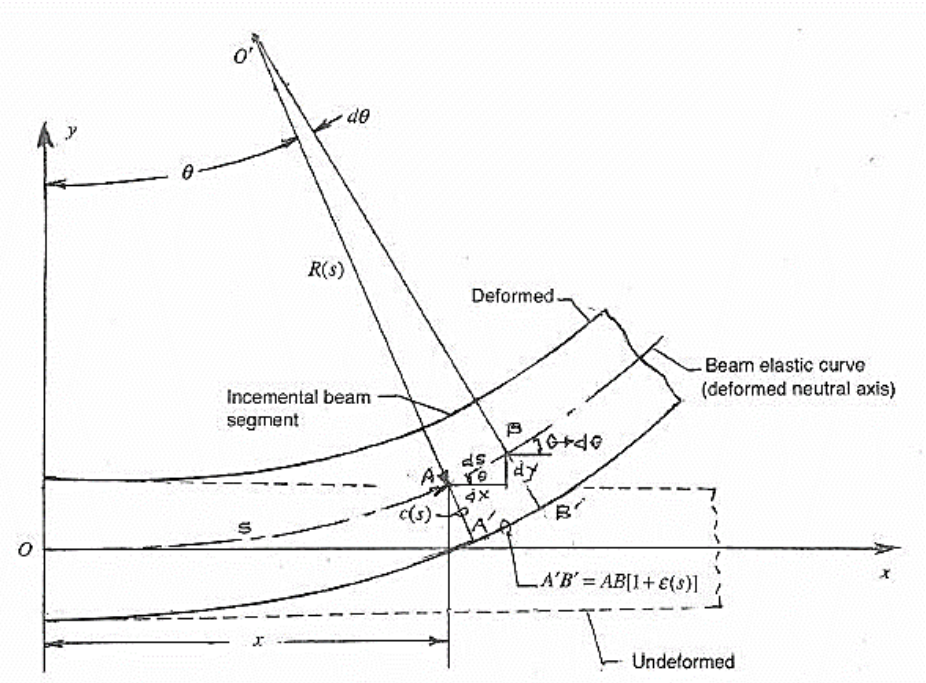

# Displacement Transfer Functions

Slope equation (recursive form):

$$tan\theta_i = (\Delta l)_i \left[ \frac{\varepsilon_{i-1} - \varepsilon_i}{c_{i-1} - c_i} + \frac{\varepsilon_{i-1} c_i - \varepsilon_i c_{i-1}}{(c_{i-1} - c_i)^2} log \frac{c_i}{c_{i-1}} \right] + tan\theta_{i-1}$$

$$\frac{Slightly\ nonuniform}{(c_{i-1} \approx c_i)} \rightarrow \frac{(\Delta l)_i}{2c_{i-1}} \left[ \left( 2 - \frac{c_i}{c_{i-1}} \right) \varepsilon_{i-1} + \varepsilon_i \right] + tan\theta_{i-1} \qquad (4)$$

$$\frac{Uniform}{(c_{i-1} = c_i = c)} \rightarrow \frac{(\Delta l)_i}{2c} (\varepsilon_{i-1} + \varepsilon_i) + tan\theta_{i-1}$$

Deflection equation (recursive form):

$$y_i = (\Delta l)_i^2 \left[ \frac{\varepsilon_{i-1} - \varepsilon_i}{2(c_{i-1} - c_i)} - \frac{\varepsilon_{i-1} c_i - \varepsilon_i c_{i-1}}{(c_{i-1} - c_i)^3} \left( c_i log \frac{c_i}{c_{i-1}} + (c_{i-1} - c_i) \right) \right] + y_{i-1} + (\Delta l)_i tan\theta_{i-1}$$

$$\frac{Slightly\ nonuniform}{(c_{i-1} \approx c_i)} \rightarrow \frac{(\Delta l)_i^2}{6c_{i-1}} \left[ \left( 3 - \frac{c_i}{c_{i-1}} \right) \varepsilon_{i-1} + \varepsilon_i \right] + y_{i-1} + (\Delta l)_i tan\theta_{i-1} \qquad (5)$$

$$\frac{Uniform}{(c_{i-1} = c_i = c)} \rightarrow \frac{(\Delta l)_i^2}{6c} (2\varepsilon_{i-1} + \varepsilon_i) + y_{i-1} + (\Delta l)_i tan\theta_{i-1}$$

# Deformed Shape Visualization

- Structure deformed shape visualization Procedure

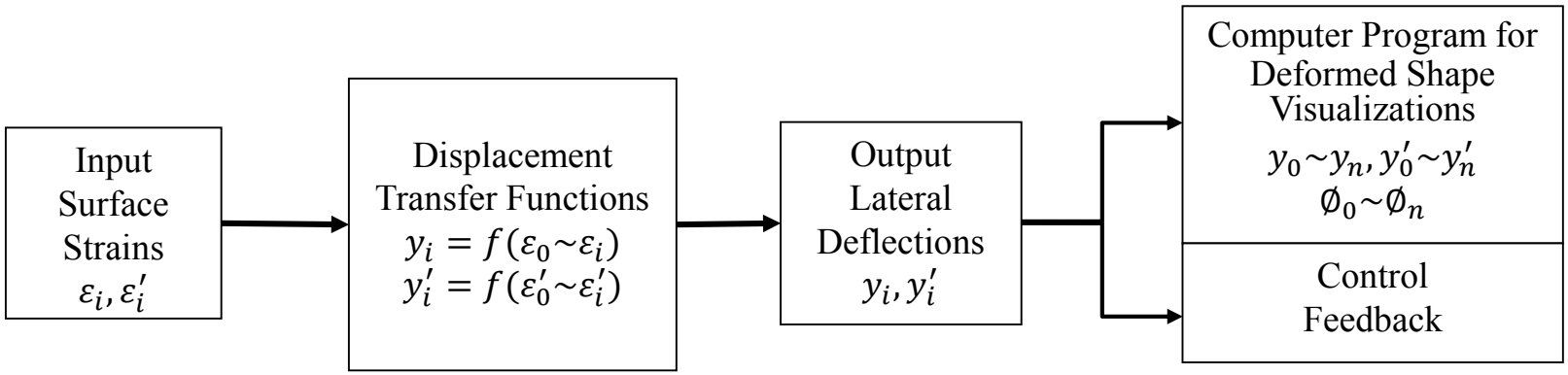


# DTFs Application

- Use four strain-sensing lines (use two strain-sensing lines if $c_i$ is known).
- Discretize the beam into *n* domains
- Determine the neutral axis (depth factor, $c_i$)

$$c_i = \frac{\varepsilon_i}{\varepsilon_i + \bar{\varepsilon}_i} h_i \qquad c_i' = \frac{\varepsilon_i'}{\varepsilon_i' + \bar{\varepsilon}_i'} h_i'$$

- Use equation (4) to calculate slope $tan\theta_i$
- Use equation (5) to calculate deflection $y_i$
- Calculate the cross sectional twisted angle

$$\phi_i = sin^{-1}\left(\frac{y_i - y_i'}{d_i}\right) \qquad (i = 0,1,2,3,\ldots,n)$$

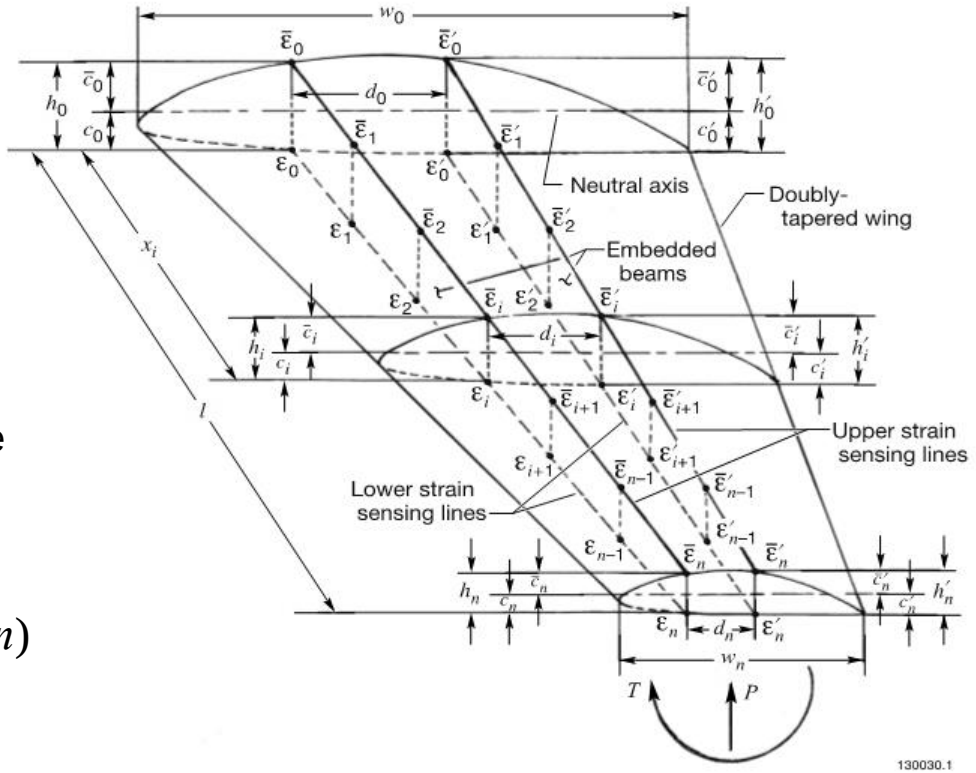

# Surface Strains for Load Case 24

- Load case 24
- Strains output from FEM model 2

Rear strain lines

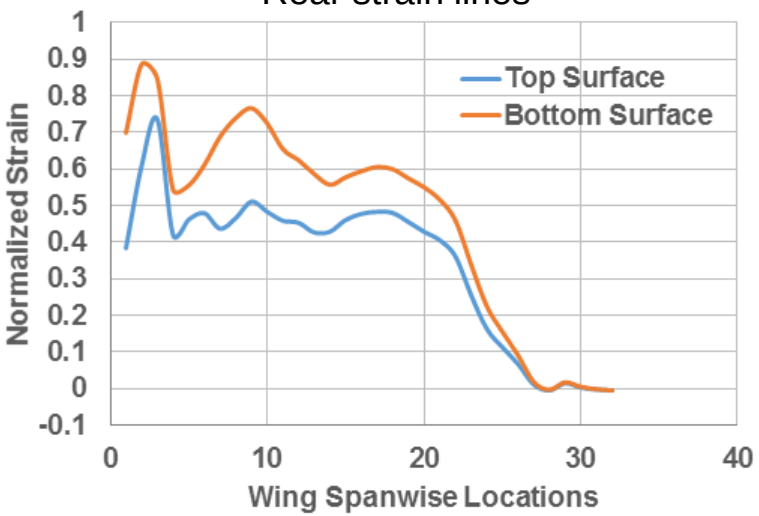


Front strain lines

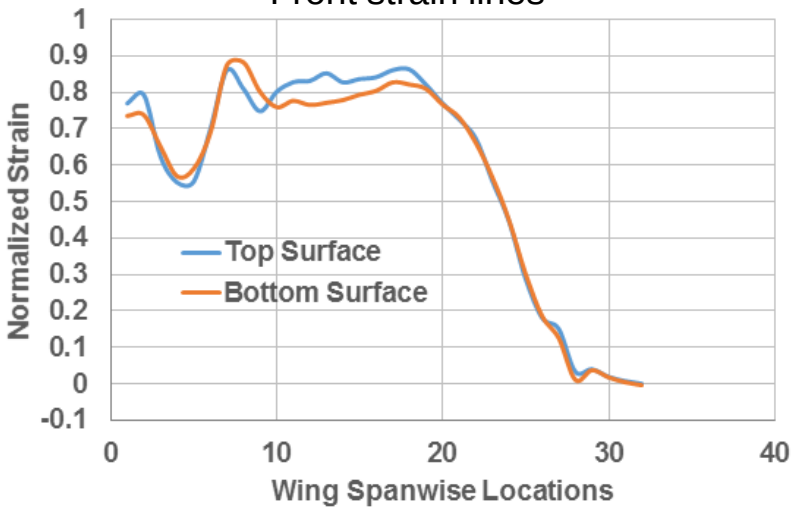

# Deflection Comparison

❖Use equation (4) to calculate deflection

Rear strain lines

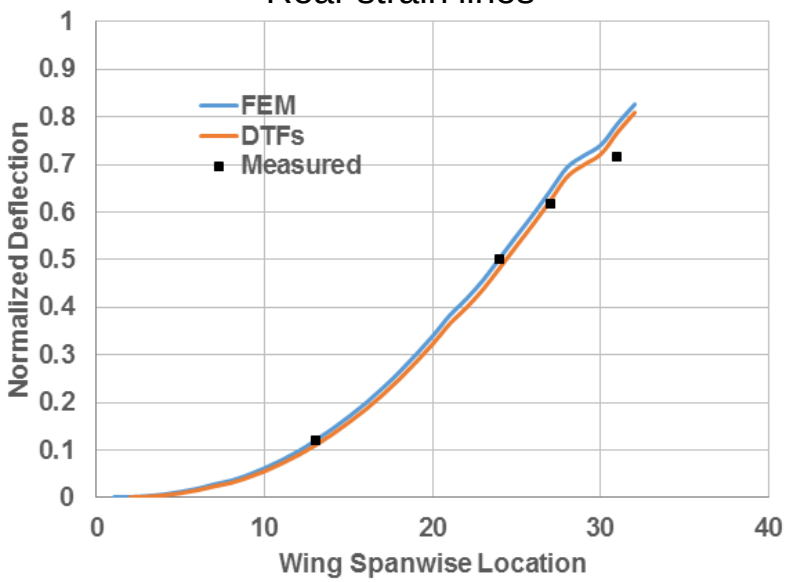


Front strain lines

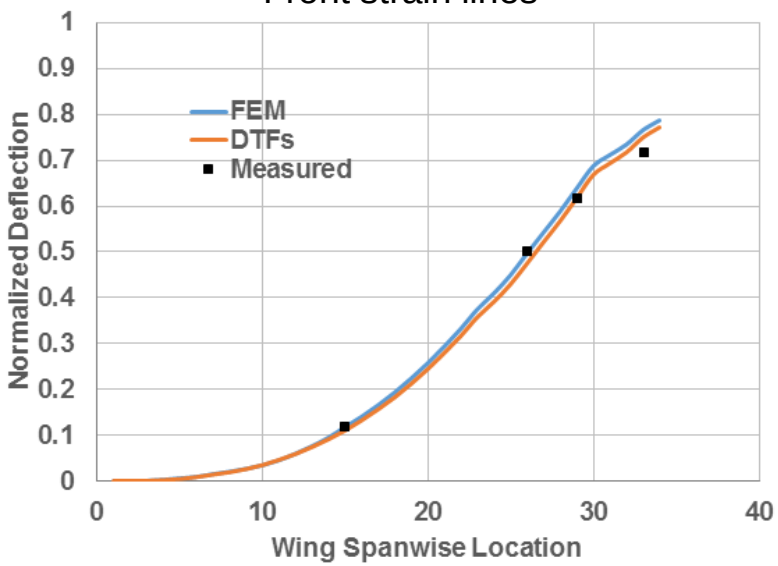

# Twist Angle Comparison

❖ Twist angle calculate from $\phi_i = sin^{-1}\left(\frac{y_i - y_i'}{d_i}\right)$

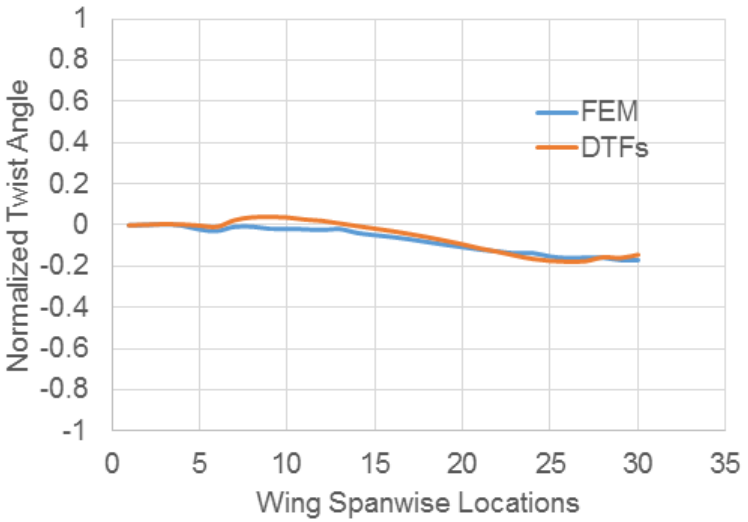


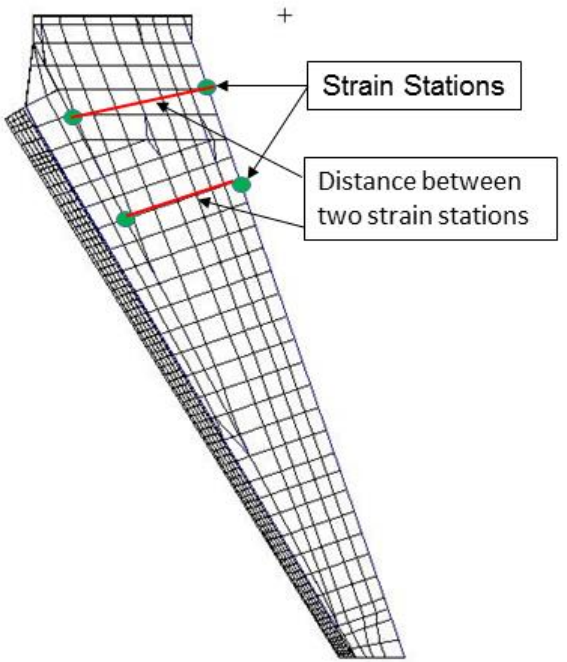

# Convergent Study

- Wing deflection base on different number of strain stations

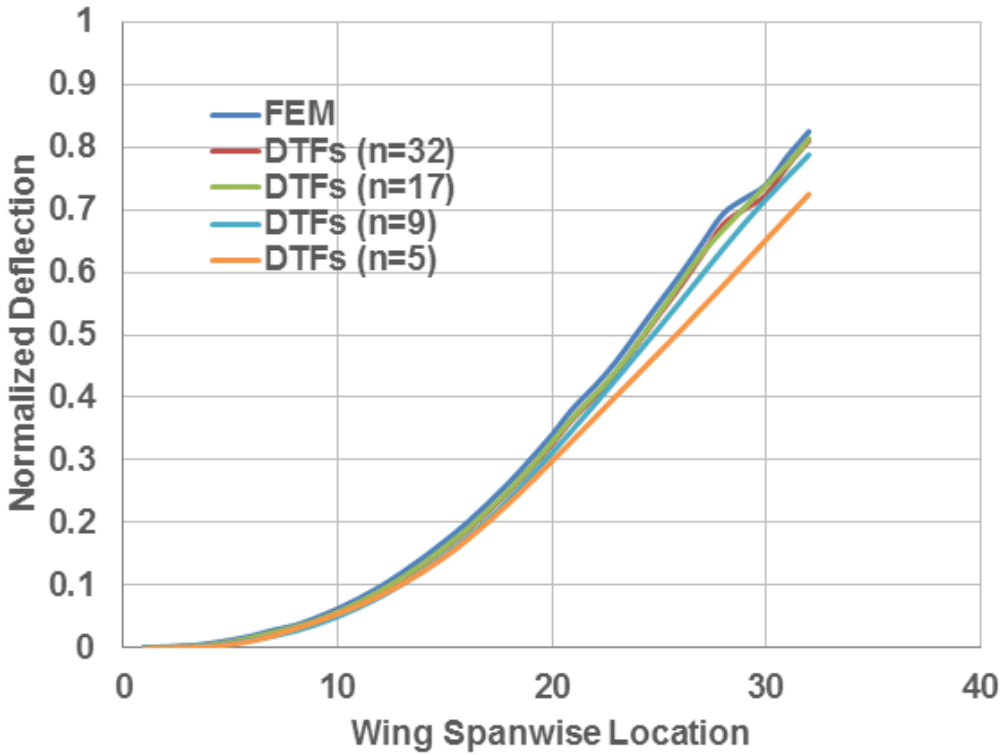

# Wing Tip Deflection Error

- Wing tip deflection error from 12% with 5 strain stations reduces to 1.6% with 17 strain stations
- Further increase number of strain stations will increase the error percentage

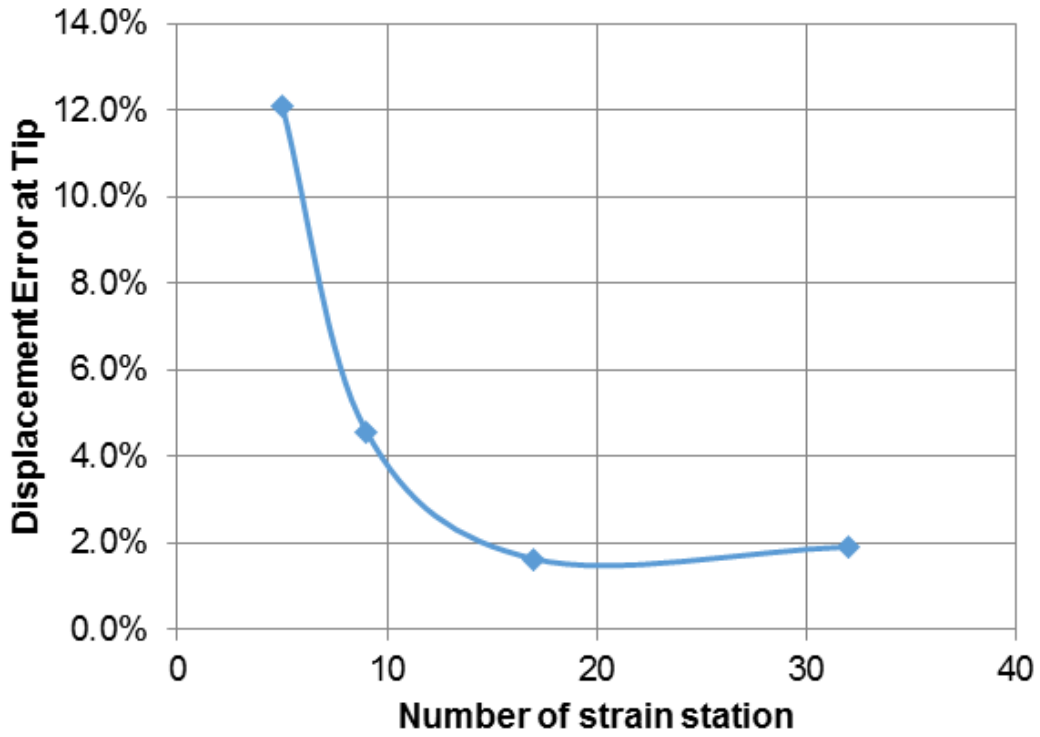

# Conclusion

- The displacement transfer functions (DTFs) were applied to the GIII swept wing for the deformed shape prediction.
- The calculated deformed shapes are very close to the correlated finite element results as well as the measured data
- The convergence study showed that using 17 strain stations, the wing-tip displacement prediction error was 1.6 percent, and that there is no need to use a large number of strain stations for G-III wing shape predictions.

# Questions